Scilight

Materials and Sustainability
https://www.sciltp.com/journals/MatSus

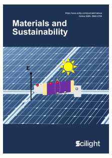

Supporting Information

Supporting Information: Hierarchical Porous Carbon-Carbon Dot Architecture as a High Energy Density Cathode for Lithium-Metal Capacitors

Gayathry Ganesh [1,2], Gokul Raj Deivendran [3], Vaishak Sunil [1,2], Izan Izwan Misnon [1,2], Chun-Chen Yang [3,4] and Rajan Jose [1,2,3,*]

[1] Center for Advanced Intelligent Materials, Universiti Malaysia Pahang Al-Sultan Abdullah, Kuantan 26300, Malaysia
[2] Faculty of Industrial Sciences and Technology, Universiti Malaysia Pahang Al-Sultan Abdullah, Kuantan 26300, Malaysia
[3] Battery Research Center of Green Energy, Ming Chi University of Technology, New Taipei City 243303, Taiwan
[4] Department of Chemical Engineering, Ming Chi University of Technology, New Taipei City 243303, Taiwan
* Correspondence: rjose@umpsa.edu.my or rjose@mcut.mail.edu.tw

Supplementary Note S1

Material Characterization

The phase composition and presence of impurities in the samples were examined using X-ray diffraction (XRD) with a Bruker D2 PHASER diffractometer (Karlsruhe, Germany) equipped with a Cu Kα radiation source (λ = 0.153 nm). Morphological analysis was carried out using a Field Emission Scanning Electron Microscope (FESEM) (JEOL, USA) coupled with Energy Dispersive X-ray Spectroscopy (EDX) for elemental composition analysis (200 kV). High-resolution imaging of f-CDs was performed using a High-Resolution Transmission Electron Microscope (HR-TEM) (JEOL JEM-2100F, Japan). The binding energies of f-CDs were investigated using X-ray Photoelectron Spectroscopy (XPS) (Sigma Probe, Thermo VGScientific, UK), utilizing an Al Kα X-ray source (1486.6 eV) and analyzed with XPSPEAK software (v. 4.1). The specific surface area (SSA) and porosity of the materials were evaluated using the Brunauer-Emmet-Teller (BET) method, based on N_2 adsorption-desorption isotherms, performed on a Micromeritics Tristar 3000 analyzer (USA). Direct current (DC) polarisation measurements were carried out in a voltage range from −2 to +2 V using a controlled in-plane sample holder (CESH; BioLogic, France) over a temperature range of 30 to 150 °C, employing an SP-300 potentiostat/galvanostat/FRA (BioLogic, France).

Electrochemical Characterizations

For the preparation of electrodes, the electrode slurry was cast onto an aluminium foil using the doctor blade method. After drying overnight in a 60 °C oven, followed by 1 h at 120 °C, the electrodes were calendared and punched into discs of 13 mm diameter with a mass loading of 1.2 $mg\cdot cm^{-2}$. These cathodes were assembled in a CR2032 coin cell with Lithium metal foil anode (purity ≥99.99%, diameter 15.8 mm, thickness ~200 µm; Biyuan Electronics, China), separated by a 16 µm thick polyethylene separator (Asahi Kasei, Japan) was employed. A liquid electrolyte of 1 M lithium hexafluorophosphate ($LiPF_6$) in a 1:1 volume mixture of ethylene carbonate (EC) and diethyl carbonate (DEC) (H_2O ~5.2 ppm, HF ~9.5 ppm; Kishida Chemical, Japan) was used. The coin cells were galvanostatically charged and discharged within the 2.0 to 4.3 V voltage range using a battery cycler (BAT-750B; AcuTech Systems, Taiwan). Electrochemical impedance spectroscopy (EIS) was performed using an Autolab PGSTAT-302N potentiostat/galvanostat (Metrohm Autolab BV, The Netherlands), covering a frequency range from 1 MHz to 10 mHz with an amplitude of 5 mV. The EIS spectra were fitted using the ZView2 software, (Version 4.1a, Scribner, LLC, North Carolina, USA) which interprets the various charge dynamics in the electrochemical system, such as diffusion rate, series resistance, polarization resistance, diffusion resistance, Warburg impedance, and double-layer capacitance, using an equivalent circuit model. In the model, each of the electrical components corresponds to a physical process occurring within the electrochemical system. A suitable model is constructed by successively choosing a minimum number of circuit components that represent a physically meaningful electrochemical system.

Supplementary Note S2

The specific capacitance (C_S) from CV was calculated by using the following equation;

$$C_S = \frac{1}{mv(E_2 - E_2)} \int_{E_1}^{E_2} i(E)dE \tag{S1}$$

where 'm' (in g) is the mass loading of the active material, 'v' ($V \cdot s^{-1}$) is the scan rate, 'V_1' and 'V_2' represent the lower and higher potential limits, and 'i(E)' is the instant current.

GCD is recorded by applying a constant current to the electrode until an upper cut-off voltage and discharging in the same current the lower cut-off voltage is attained. The C_s from GCD was calculated by;

$$C_S = \frac{I\Delta t}{mV} \tag{S2}$$

where 'I' is the current applied, 'Δt' is the discharge time and 'V' is the working potential.

The energy density and power density were calculated using the following equation;

$$E_d = C_s V \tag{S3}$$

$$P_d = \frac{E_d}{t_d} \tag{S4}$$

where t_d is the discharge time

The circuit modelling of the impedance data was done using Zview software with a minimum number of physically meaningful parameters.

The electrochemical active surface area is calculated using equation (7) with the imaginary impedance at 0.01 Hz from the Nyquist plot [1].

$$S_E = \frac{C_{dl}}{C_d}$$

where $C_{dl} = (2\pi m f Z'')^{-1}$ and $C_d = 0.002$ mF.cm^{-2} for carbonaceous materials.

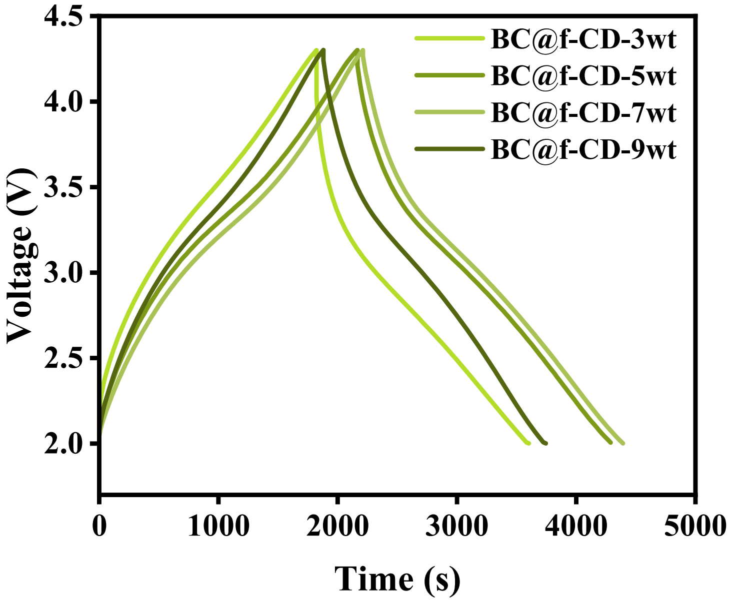

Figure S1. A comparative GCD plot used to optimize the f-CD concentration in BC.

Table S1. Literature comparing the BET surface area of materials before and after the addition of CDs.

Material	Without CDs	With CDs	Reference
Electrostatic densified AC	3245	3359	[2]
CuS	23	111	[3]
Fe_3O_4	88	290	[4]
Bi/BiOI	9.6	24.1	[5]
BTPAC	773.9	799.0	[6]

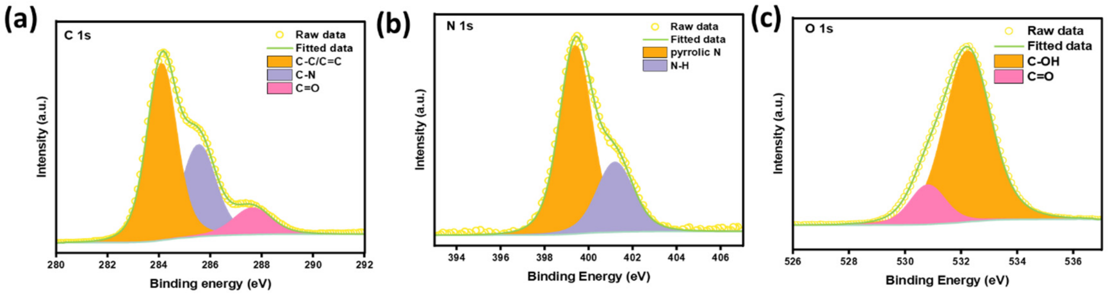

Figure S2. Deconvoluted XPS spectra of (**a**) C1s, (**b**) N1s and (**c**) O1s.

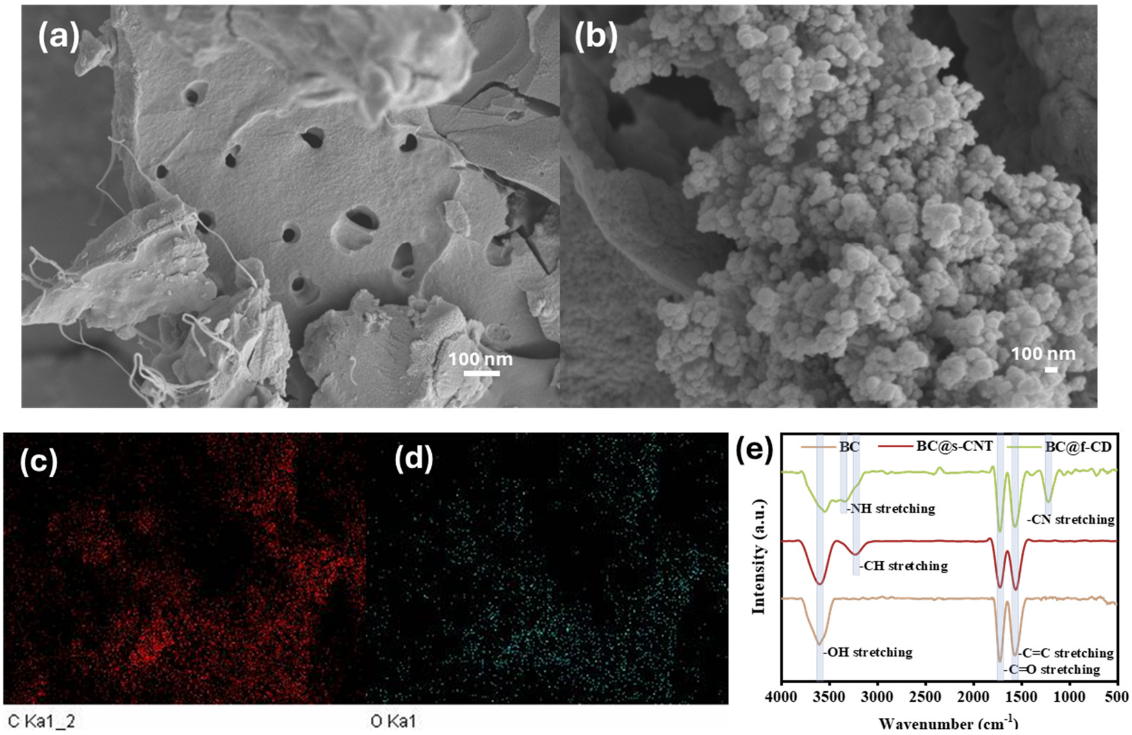

Figure S3. SEM images of (**a**) BC@s-CNT and (**b**) BC@f-CD. The f-CD particles appear to be aggregated due to the SEM resolution limitation. EDX mapping of BC for (**c**) carbon and (**d**) oxygen, (**e**) comparative FTIR of BC, BC@s-CNT and BC@f-CD.

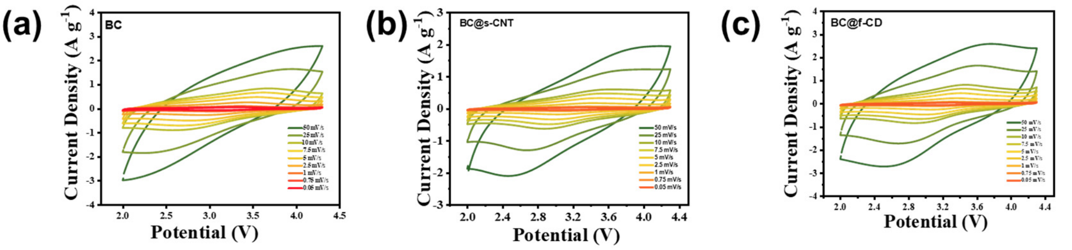

Figure S4. CV plots at different scan rates for (a) BC, (b) BC@s-CNT, and (c) BC@f-CD.

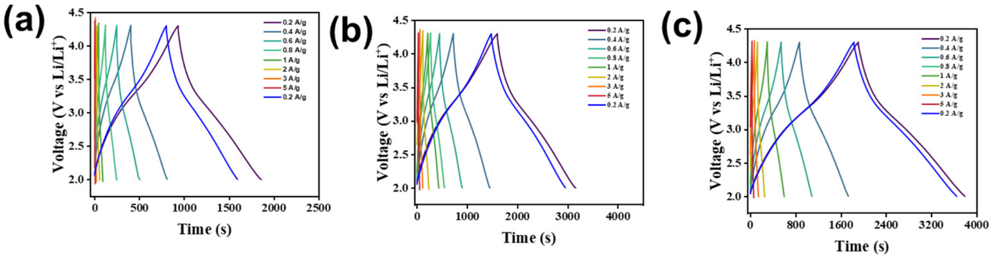

Figure S5. GCD plots at different current densities for (**a**) BC, (**b**) BC@s-CNT, and (**c**) BC@f-CD.

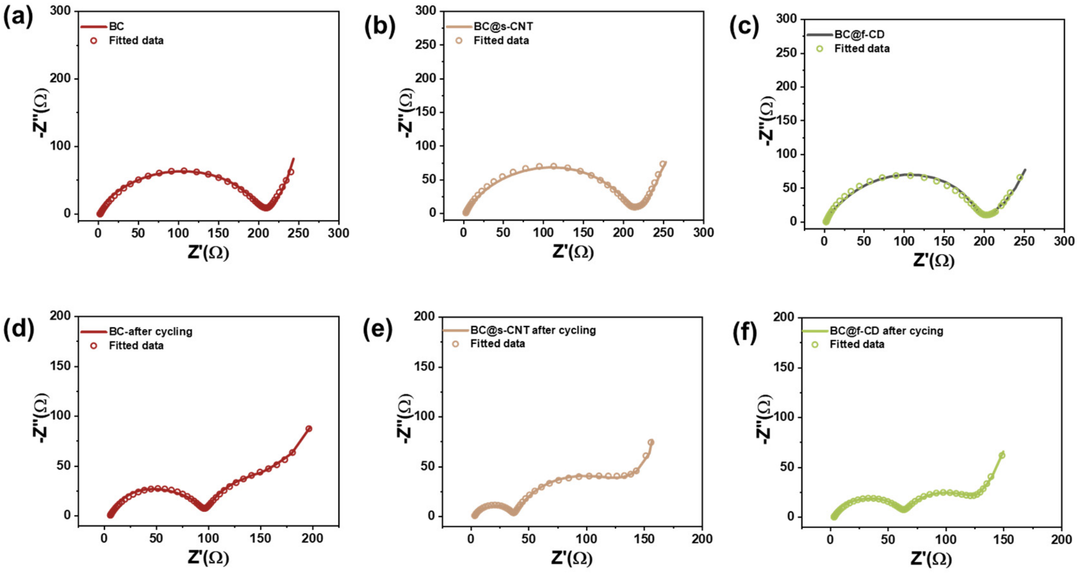

Figure S6. EIS fitted data for (**a**) BC, (**b**) BC@s-CNT, and (**c**) BC@f-CD before cycling. EIS fitted data for (**d**) BC, (**e**) BC@s-CNT, and (**f**) BC@f-CD after cycling.

References

1. Lee, S.P., Ali, G.A.M.; Hegazy, H.H.; et al. Optimizing Reduced Graphene Oxide Aerogel for a Supercapacitor. *Energy Fuels* **2021**, *35*, 4559-4569.
2. Jiang, Y.; Li, J.; Jiang, Z.; et al. Large-surface-area activated carbon with high density by electrostatic densification for supercapacitor electrodes. *Carbon* **2021**, *175*, 281–288.
3. Quan, Y.; Wang, G.; Lu, L.; et al.; High-performance pseudo-capacitor energy storage device based on a hollow-structured copper sulfide nanoflower and carbon quantum dot nanocomposite. *Electrochimica Acta* **2020**, *353*, 136606.
4. Yang, P.; Zhu, Z.; Chen, M.; et al. Microwave-assisted synthesis of xylan-derived carbon quantum dots for tetracycline sensing. *Opt.Mater.* **2018**, *85*, 329–336.
5. Zhao, C.; Zhao, Z.; Liang, Y.; et al. Bi/BiOI/carbon quantum dots nano-sheets with superior photocatalysis. *RSC Adv.* **2023**, *13*, 30520–30527.
6. Rong, C.; Liao, C.; Chen, Y.; et al. High-performance supercapacitor electrode materials from composite of bamboo tar pitch activated carbon and tannic acid carbon quantum dots. *J. Energy Storage* 2024, **95**, 112657.